Does DCE-MRI Have a Metabolic Dimension?

Martin M. Pike[1], Mohan L. Jayatilake[1], Xiaoyan Wang[2], Merryl R. Lobo[1], Xin Li[1], Matthias C. Schabel[1], William D. Rooney[1], Dale J. Christensen[3], Jerry D. Glickson[4], Rosalie C. Sears[2], Wei Huang[1], and Charles S. Springer[1]

[1]Advanced Imaging Research Center, Oregon Health & Science University, Portland, Oregon, United States, [2]Molecular and Medical Genetics, Oregon Health & Science University, Portland, Oregon, United States, [3]Oncotide Pharmaceuticals, Research Triangle Park, North Carolina, United States, [4]Radiology, University of Pennsylvania, Philadelphia, Pennsylvania, United States

Introduction: Malignant tumor metabolism is currently receiving intense scrutiny (1,2). Biomedical imaging assesses this mainly *via* PET (3) and, more recently, hyperpolarized ^{13}CMRSI (4). Although [Dynamic-Contrast-Enhanced] DCE-MRI is increasingly used for cancer (5), it is widely thought restricted to microvascular property and extracellular space determinations. However, it has been recently discovered that the mean intracellular water lifetime [τ_i] is an inverse measure of ongoing cellular metabolic fluxes (6). Though the τ_i biomarker is artificially held effectively zero when DCE-MRI data are analyzed with the tracer pharmacokinetic paradigm, it is determined when equilibrium trans-cytolemmal water exchange kinetics are included (7). This suggests that DCE-MRI can have a heretofore unrecognized metabolic dimension. We have studied a genetically modified murine spontaneous breast cancer model. This is RFS-Myc:NeuNt:Blg-Cre; a cross of a mouse expressing a Cre-inducible homozygous c-Myc knock-in gene [ROSA26 locus] with an individual carrying a heterozygous Cre-inducible activated Her2/Neu knock-in at its endogeneous oncogene, and with a Blg-Cre transgenic mouse for mammary specific Cre expression to drive c-Myc and NeuNT. Four to twelve weeks after their first pregnancy lactation to stimulate Blg-Cre, parous females develop mammary tumors morphologically and histologically similar to human breast cancer. The malignancy is driven by activated Her2 signaling and de-regulated c-Myc expression, with the c-Myc protein near human tumor levels (8,9).

Methods: An approximately seven month old 35 g female with a right gland tumor was anesthetized [ketamine/xylazine; maintained with isoflurane] and cradled supine in an 11.74T/31 cm MRI instrument (Bruker). Body temperature was maintained and respiration monitored. A spoiled GE-FLASH DCE-MRI acquisition [TR/FA; 40 ms/27°] used a 7.2 cm body RF transmit coil and a 2 cm surface receive coil over the tumor. The slice thickness was 750 μm, the nominal in-plane spatial resolution (195 μm)^2, and the temporal resolution 5 s. Just over one minute into the 13 minute acquisition, a dose [0.15 mmol/kg] of ProHance [75 μL of 71 mM] contrast reagent (CR) was delivered in 4.5 s through a tail vein cannula, with a 12 s 200 μL saline chase. The arterial input function was determined by blind estimation (10) from the brain tumor tissue response to an identical injection in another mouse. For the breast tumor tissue response, the Fast-Exchange-Regime-allowed form of the Shutter-Speed pharmacokinetic analysis was used. This assumes the ^1H_2O T_1 remains single-valued: *i.e.*, there is one tissue ^1H_2O signal (7).

Results: Two DCE-MRI biomarkers are analyzed, τ_i and K^{trans}, primarily a tumor capillary CR extravasation rate constant (7). **Figure 1** shows axial tumor parametric maps superimposed on gray scale T_1-weighted whole body image slices. The view is from the inferior perspective [the right gland tumor is image left]: anterior is up. The image slice shown is the most superior of four contiguous planes passing through the tumor, which was ~5 mm in diameter. The **left** and **right** panels show K^{trans} and τ_i maps, respectively, the color scales are given. The **upper** panels show the heterogeneity of the spontaneously developed tumor. The values of K^{trans} and τ_i each vary by a factor of five or more across the lesion. Comparison of the K^{trans} and τ_i maps shows aspects of the negative spatial correlation often reported (11-14): in many regions where K^{trans} is relatively large [*e.g.*, anterior periphery] τ_i is relatively small, and *vice-versa*. This is thought not a parameter interdependence numerical correlation (7). Where capillaries are more permeable, metabolism (specifically trans-membrane ion and osmolyte cycling) is faster. The **lower** panels show analogous maps of the same tumor after 10 days of o.d. injection [IP] of 5 mg/kg OP449, a therapeutic peptide mimetic that re-activates the crucial tumor suppressor enzyme protein phosphatase 2A [PP2A] by inhibiting its SET oncoprotein inhibitor (15). Though the tumor volume increased 1.3 fold here, this is much less than mice with no therapy [5.4 fold; n = 12] and the pharmacokinetic parameters show pronounced changes suggestive of therapeutic efficacy. K^{trans} decreases significantly with therapy, while τ_i increases. Thus, they are negatively correlated in this way also.

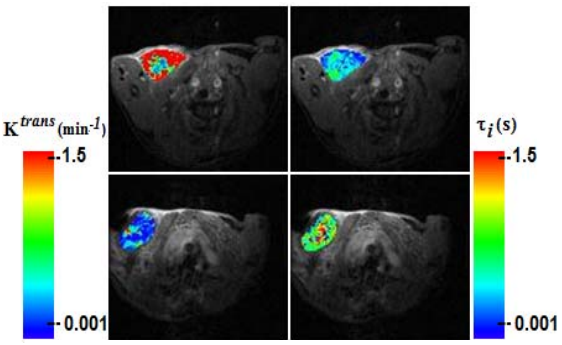

Figure 1. Parametric maps.

Since we have two responsive biomarkers, we can inspect DCE-MRI in a two dimensional fashion (16). **Figure 2** shows pixel-by-pixel 2D scatter plots [K^{trans} ordinate, τ_i abscissa] of the Fig. 1 image slices. The **upper** panel depicts the situation before therapy. The accumulation of some points at K^{trans} = 3 min^{-1} is simply the upper bound of the analytical K^{trans} iteration. The eye discerns instances of spatial parameter correlation [Fig. 1 upper] when simple numerical correlation is not evident [Fig. 2 upper]. The **lower** Fig. 2 panel shows the situation after therapy. Large changes are obvious. The cluster center of mass coordinates [K^{trans}, τ_i] go from approximately [0.7 min^{-1}, 0.4 s] to approximately [0.2 min^{-1}, 0.8 s] post-therapy: each coordinate changes by a factor of two or more. K^{trans} has been found to decrease with almost every anti-cancer drug tested (5). The τ_i magnitudes seen here are very reasonable (7).

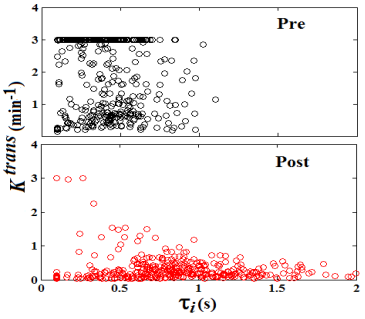

Figure 2. Scatter plots.

Discussion: The c-Myc gene product is a transcription factor heavily involved in metabolic signaling (17). This tumor model has a human-like level of c-Myc activity, and the OP449 peptide is designed to counteract this through re-activation of PP2A, a direct negative regulator of c-Myc phosphorylation and activity (18,19). So, it is sensible that we see a τ_i change upon OP449 therapy consistent with a significant metabolic flux decrease. This is encouraging that DCE-MRI does have a useful metabolic dimension: τ_i is the parameter most directly pertinent to cancer. It can arise directly from the tumor cells.

Grant Support: NIH: UO1-CA154602; RO1-NS40801; RO1-CA100855; RO1-CA129040, DOD: BC061306, Komen: BCTR0706821.

References: **1.** Ward, Thompson, *Can Cell*, **21**:297(2012). **2.** Dang, *Can Res*, **70**:859(2010). **3.** Vander Heiden, *et al*, *Sci*, 324:1029(2009). **4.** Larson, *et al*, *PISMRM* **20**:61(2012). **5.** O'Connor, *et al*, *Nat Rev Clin Oncol* **9**:167(2012). **6.** Zhang, *et al*, *Biophys J* **101** 2833(2011). 7. Li, *et al*, *JMR* **218**:77(2012). **8**. Wang, *et al*, *Can Res*, **71**:925(2011). **9.** Zhang, *et al*, *PNAS* **109**:2790(2012). **10.** Schabel, *et al*, *Phys Med Biol* **55**:4783 (2010). **11.** Huang, *et al*, *PISMRM* **20**:452(2012). **12.** Li, *et al*, *PISMRM* **19**:3115(2011). **13.** Kim, *et al*, *JMRI* **26**:1607(2007). **14.** Yankeelov, *et al*, *NMR Biomed* **18**:173(2005). **15.** Christensen, *et al*, *Blood* **118**:4150(2011). **16.** Rajendran, *et al*, *Clin Can Res* **10**:2245(2004). **17.** DeBerardinis, *et al*, *Cell Metabol* **7**:11(2008). **18.** Arnold, Sears, *Mol Cell Biol* **26**:2832(2006). **19.** Yeh, *et al*, *Nat Cell Biol* **6**:308(2004).